© 2016. Published by The Company of Biologists Ltd | Journal of Experimental Biology (2016) 219, 404-411 doi:10.1242/jeb.127928

RESEARCH ARTICLE

XROMM analysis of rib kinematics during lung ventilation in the green iguana, *Iguana iguana*

Elizabeth L. Brainerd*, Sabine Moritz and Dale A. Ritter

ABSTRACT

The three-dimensional rotations of ribs during breathing are typically described as bucket-handle rotation about a dorsoventrally oriented axis, pump-handle rotation about a mediolateral axis, and caliper rotation about a rostrocaudal axis. In amniotes with double-headed ribs, rib motion is constrained primarily to one degree-of-freedom (DOF) rotation about an axis connecting the two rib articulations. However, in Squamata, the ribs are single headed and the hemispherical costovertebral joints permit rotations with three DOF. In this study, we used X-ray reconstruction of moving morphology (XROMM) to quantify rib rotation during deep breathing in four green iguanas. We found that rib rotation was strongly dominated by bucket-handle rotation, thus exhibiting nearly hinge-like motion, despite the potential for more complex motions. The vertebral and sternal segments of each rib did not deform measurably during breathing, but they did move relative to each other at a thin, cartilaginous intracostal joint. While standing still and breathing deeply, four individual iguanas showed variability in their rib postures, with two breathing around a highly inflated posture, and two breathing around a posture with the ribs folded halfway back. Bucket-handle rotations showed clear rostrocaudal gradients, with rotation increasing from the third cervical to the first or second dorsal rib, and then decreasing again caudally, a pattern that is consistent with the intercostal muscles in the rostral intercostal spaces being the primary drivers of inspiration. The constrained, primarily bucket-handle rotations observed here during breathing do not help to explain the evolution of permissive, hemispherical costovertebral joints in squamates from the more constrained, double-headed rib articulations of other amniotes.

KEY WORDS: Squamata, Lizard, Breathing, Biomechanics, X-ray, Costovertebral joint, Sternocostal joint, Sternal rib, Vertebral rib

INTRODUCTION

Breathing may seem like a simple behavior, but in fact the morphology and mechanics of the amniote thorax are enormously complex. Lung ventilation by aspiration breathing poses a fundamental biomechanical problem: muscles do work only while shortening, but inhalation requires expansion of the thorax to draw air down into the lungs. How is muscle shortening converted into thoracic expansion?

In amniotes, the solution takes two forms: skeletal lever systems and special arrangements of muscle fibers, such as the domed shape of the mammalian diaphragm or the hepatic piston mechanisms of crocodilians. The ribs and intercostal muscles form a set of skeletal lever systems that convert intercostal muscle shortening into lateral and cranial motion of the ribs. This costal aspiration system appears to be the primitive ventilation mechanism for amniotes (Brainerd and Owerkowicz, 2006). Accessory diaphragm-like arrangements have evolved independently in mammals, turtles and crocodilians, but in all extant amniotes except turtles, rib motions contribute to lung ventilation, suggesting that costal aspiration is primitive for amniotes (Brainerd, 2015; Brainerd and Owerkowicz, 2006).

Squamates retain this primary reliance on costal aspiration for lung ventilation; hence, lizards and snakes are good subjects for the study of rib kinematics. Motions of their ribs tend to be large, particularly in iguanians, a group that concentrates costal motions into a small number of ribs in the rostral part of the trunk (Carrier, 1989). The costovertebral joints of squamates are simple, with a cup-shaped articular surface on the head of the rib that articulates with a hemispherical articular surface on the vertebral centrum (Hoffstetter and Gasc, 1969; Romer, 1956). The singled-headed (unicapitate) rib morphology and simple costovertebral joints of squamates appear to be derived from a primitive bicapitate condition for Amniota. All other amniote groups, including Rhynchocephalia, the sister group to squamates, have bicapitate ribs that articulate with the vertebral column via two separate articulations, the diapophysis and the parapophysis. In *Sphenodon*, the only extant rhynchocephalian, the most rostral pair of ribs is bicapitate, and the remainder maintain an elongate, hemi-ellipsoidal articulation with the vertebrae. From *Sphenodon* and developmental evidence, it is clear that the single articulation with the vertebrae in *Sphenodon* and squamates is a synapophysis, formed by fusion of the diapophysis and the parapophysis, rather than loss of one of them (Hoffstetter and Gasc, 1969; Romer, 1956).

Given this relatively simple, unicapitate rib morphology, it is not possible to predict, *a priori*, the kinematics of squamate ribs during lung ventilation. The hemispheric costovertebral joints in squamates could allow motions in all three potential rotational degrees of freedom (DOF). The three potential rotations of ribs have been described as bucket-handle, pump-handle and caliper rotation (Fig. 1). Various authors have placed the coordinate system describing these motions somewhat differently, such as oriented to the body axes or oriented to some feature of the costovertebral joints, so the definitions of these rotations have not always been consistent (Osmond, 1985). For this study, and to facilitate comparison with other species, we have chosen to orient the coordinate system to the body axes, such that rotation about a rostrocaudal axis is caliper motion (Fig. 1A), rotation about a dorsoventral axis is bucket-handle motion (Fig. 1B) and rotation about a mediolateral axis is pump-handle motion (Fig. 1C). Squamate ribs may potentially rotate around all of these axes, given the permissive hemispherical shape of the costovertebral joints.

Department of Ecology and Evolutionary Biology, Brown University, Providence, RI 02906, USA.

*Author for correspondence (elizabeth_brainerd@brown.edu)

Received 6 July 2015; Accepted 16 November 2015

Journal of Experimental Biology

Journal of Experimental Biology (2016) 219, 404-411 doi:10.1242/jeb.127928

List of symbols and abbreviations

C1–C4	cervical ribs 1–4
CT	computed tomography
DOF	degrees of freedom
Ig01–Ig05	*Iguana* individuals 1–5
JCS	joint coordinate system
S1–S4	sternal ribs 1–4
V1–V4	vertebral ribs 1–4
XROMM	X-ray reconstruction of moving morphology
ZYX	rotation order for JCS Euler angles

We selected the green iguana, *Iguana iguana*, for this study because this species grows to large body sizes and exhibits large rib motions in the axillary region during breathing (Movie 1). Green iguanas have four pairs of ribs that connect to both the vertebral column and the sternum (Fig. 1D). These four ribs have two segments: a dorsal, osseous vertebral rib segment and a ventral, cartilaginous sternal rib segment. It is unknown whether the two rib segments move relative to each other, or whether the whole rib may act as a single object during lung ventilation. It is also possible that the cartilaginous sternal rib may bend along its length during ventilation. Therefore, this study tested three hypotheses: (1) the sternal ribs deform during lung ventilation; (2) the vertebral and sternal ribs move relative to each other, with the motion occurring at the putative intracostal joint (Fig. 1D); and (3) unicapitate costovertebral joints allow complex motions with three rotational DOF during lung ventilation. XROMM (X-ray reconstruction of moving morphology) yields data on both the shape and motion of skeletal elements (Brainerd et al., 2010), and will be used here to measure shape and motion of the vertebral and sternal ribs and associated vertebrae and sternum of green iguanas during deep breathing.

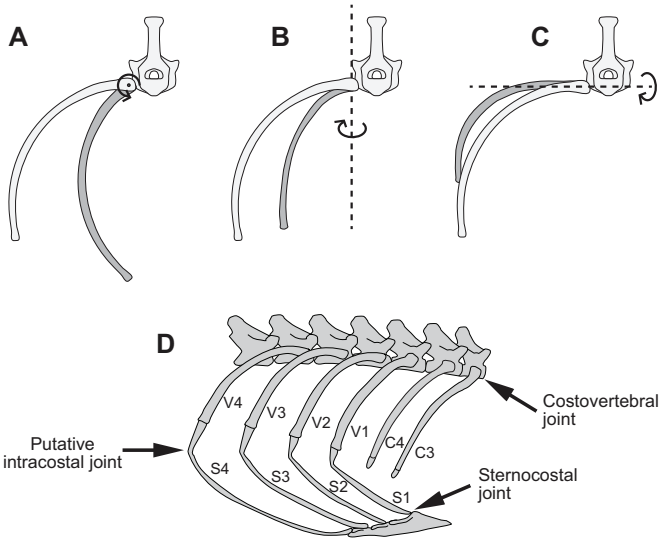

Fig. 1. Rotations at the costovertebral joints, and structure of the rib cage in *Iguana iguana*. Motion at the costovertebral joints is typically described as a combination of three rotations: (A) caliper rotation about a rostrocaudal axis; (B) bucket-handle rotation about a dorsoventral axis; and (C) pump-handle rotation about a mediolateral axis. (D) Green iguanas have four cervical ribs (C1–C4; first two not shown here), and four dorsal ribs with direct connections to the sternum. The dorsal ribs have vertebral segments (V1–V4) and sternal segments (S1–S4), connected via putative intracostal joints (the 'elbow' of the rib).

MATERIALS AND METHODS

Five adult green iguanas, *Iguana iguana* (Linnaeus 1758), were used in this study. The first individual, Ig01, was valuable for methods development but did not yield useful data; only data from Ig02–Ig05 are reported here. The animals were all large adults with body masses ranging from 2.6 to 4.6 kg. All but one (Ig03) were male. All animal care and experimental procedures were approved by the Institutional Animal Care and Use Committee of Brown University.

We used a combination of marker-based and markerless XROMM to create 3D animations of the vertebral column, ribs and sternum. Prior publications give details of marker-based XROMM methods (Brainerd et al., 2010) and markerless Scientific Rotoscoping (Gatesy et al., 2010). Briefly, for marker-based XROMM, we surgically implanted, under isoflurane anesthesia, a minimum of three metal markers in each bone. We used three different marker types, depending on the bone. Ribs were marked with 'beads on posts': 1 mm tantalum beads (Baltec, Los Angeles, CA, USA) with holes laser-drilled into them, mounted on short (2–3 mm long) segments of 000 sized (0.25 mm diameter) insect pins. The sternum was marked with 0.8 mm solid tantalum beads (Baltec). A hand drill with diameter matching the marker type, 0.25 or 0.8 mm, was used to drill a small hole in the bone. Beads on posts and solid beads were press-fitted into the drilled holes. The vertebrae were marked with tungsten carbide conical markers (Kambic et al., 2014).

Markers were spaced as far apart as possible to maximize the accuracy of rigid-body bone animations (Brainerd et al., 2010). The iguanas usually fed and behaved normally a day after surgery, but were allowed to recover for at least 1 week before the start of data recording. They received a dose of analgesic immediately before and after surgery and continued to feed and behave normally with no further pain medication.

X-ray videos were collected either with biplanar C-arm fluoroscopes (Brainerd et al., 2010) or with custom-made biplanar videoradiography equipment (Miranda et al., 2011). Videos were recorded at 60–125 frames s^{-1}, with 70–90 kV and 4–20 mA (C-arms) or 100–200 mA (videoradiography).

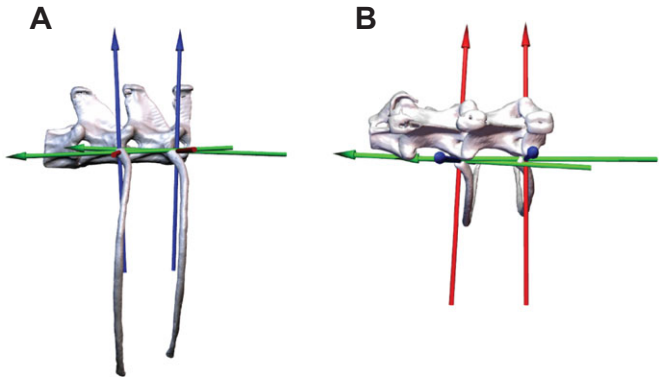

Fig. 2. Costovertebral joint coordinate system. (A) Lateral view and (B) dorsal view. This joint coordinate system (JCS) measures rotations and translations of the vertebral rib relative to the vertebra. Axis orientations were set such that rotation about the *Z*-axis (blue) is bucket-handle motion, rotation about the *Y*-axis (green) is caliper motion, and rotation about the *X*-axis (red) is pump-handle motion. To provide a consistent zero position for this JCS, vertebral ribs were manually positioned such that most of the rib lies in a transverse plane, with the neck oriented tangential to a horizontal plane at the height of the costovertebral joint. All rotations were measured relative to this zero (even though this is not a natural pose, it is a reproducible pose for all individuals).

Journal of Experimental Biology (2016) 219, 404-411 doi:10.1242/jeb.127928

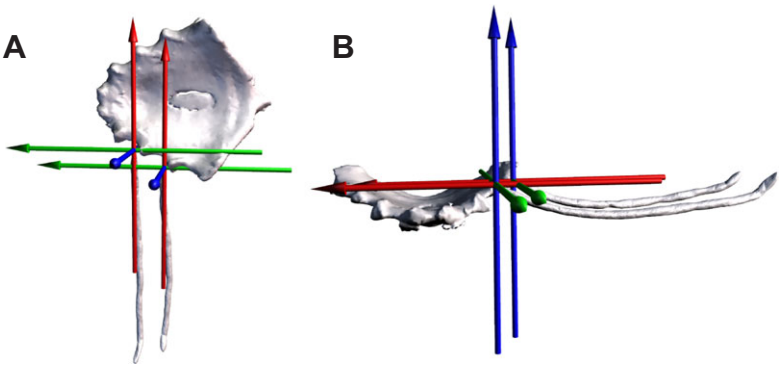

Fig. 3. Sternocostal JCS. (A) Dorsal view and (B) caudal view. This JCS measures rotations and translations of the sternal rib relative to the sternum. Axis orientations were set such that rotation about the *Z*-axis (blue) is bucket-handle, rotation about the *Y*-axis (green) is caliper (depression–elevation), and rotation about the *X*-axis (red) is long-axis rotation. To provide a consistent zero position for this JCS, sternal ribs were manually positioned such that the long axis of the sternal rib lies perpendicular to the long axis of the body, and the proximal and distal tips of the rib lie in the same horizontal plane at the height of the sternocostal joint. All rotations were measured relative to this zero (even though this is not a natural pose, it is a reproducible pose for all individuals).

After video data collection, the animals were killed by an overdose of pentobarbital, and computed tomography (CT) scans of the trunks were collected at Rhode Island Hospital (Philips Medical System, Best, The Netherlands; 80 kV, variable mA, 0.625 mm slice thickness). OsiriX (Pixmeo, Geneva, Switzerland) was used to create polygonal mesh surface models of the marked bones and metal markers, resulting in a 3D mesh surface model of each bone and the positions of the markers relative to the bones.

The X-ray video and CT scan data collected and analyzed for this study are available from the X-ray Motion Analysis Portal (xmaportal.org).

Marker tracking and XROMM animation

X-ray videos were processed with the XrayProject program (available from xromm.org) in Matlab (The MathWorks, Natick, MA, USA) to create rigid-body transformation for marker-based XROMM and undistorted video sequences for Scientific Rotoscoping (Brainerd et al., 2010; Gatesy et al., 2010). Marker coordinates were filtered with a Butterworth low-pass filter (cut-off frequency, 1 Hz), and rigid-body transformations were calculated. Rigid-body transformations for the marker sets were then applied to the 3D bone models from CT scans in Maya animation software (Autodesk, San Rafael, CA, USA). For Scientific Rotoscoping, we used hierarchical models for most of the animated bones (Gatesy et al., 2010). We animated five breathing cycles from full inhalation to the next full inhalation for all four individuals. The first dorsal rib was animated for all individuals, with various combinations of additional cervical and dorsal ribs among the individuals.

Joint coordinate systems

From the 3D animations created in Maya, we extracted bone kinematics using joint coordinate systems (JCSs). In Maya, JCSs were established for three different joints per rib, measuring translations and rotations of the vertebral rib relative to the vertebra (costovertebral joint; Fig. 2), the sternal rib relative to the sternum (sternocostal joint; Fig. 3), and the sternal rib relative to the vertebral rib (intracostal joint; Fig. 4). These JCSs describe motion as Euler angles, with the rotation order set as *ZYX*. Following best practice for *ZYX* rotation order, the axes were oriented such that rotation around the *Z*-axis describes the largest range of motion, followed by the *Y*-axis and *X*-axis (Brainerd et al., 2010). For the vertebral and sternal ribs, preliminary analysis showed that their largest motions were bucket-handle rotations, so the *Z*-axis was oriented dorsoventrally to capture this rotation (Figs 2, 3).

To provide consistent starting positions for the JCSs, all bones were arranged in reference poses prior to animation. These poses do not necessarily reflect naturally occurring bone positions, but rather were consistent and repeatable for comparison of rib postures among the four individuals (Baier et al., 2013). Vertebral ribs were positioned such that most of the rib lies in a transverse plane (Fig. 2). The neck was oriented tangential to a horizontal plane at the height of the costovertebral joint. In this reference pose (zero position), the vertebral rib lies perpendicular to the long axis of the body. Polarity of the rotations is determined by the right-hand rule; exhalation is associated with decreasing (more negative) bucket-handle angles and inhalation with increasing (less negative) bucket-handle angles (rotation about the *Z*-axis).

The zero position of sternal ribs was similar to that of vertebral ribs. In the zero position, the long axis of the sternal rib lies perpendicular to the long axis of the body (Fig. 3). The rib itself lies mostly in a transverse plane. Proximal and distal tips of the rib lie in the same horizontal plane at the height of the sternocostal joint.

For the intracostal joint, the *X*-axis was oriented along the long axis of the sternal rib, and the *Z*-axis was oriented to lie in the plane formed by the vertebral rib (Fig. 4). Rotation around the *Z*-axis indicates abduction–adduction of the sternal rib segment, relative to

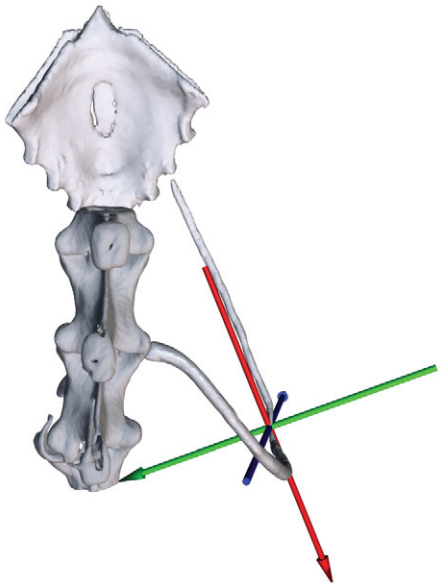

Fig. 4. Intracostal joint coordinate system. This JCS measures rotations and translations of the sternal rib relative to the vertebral rib. Axis orientations were set such that rotation about the *Z*-axis (blue) is abduction–adduction of the sternal rib segment relative to the vertebral rib, rotation about the *Y*-axis (green) is depression–elevation, and rotation about the *X*-axis (red) is long-axis rotation. Polarity of the rotations is determined by the right-hand rule. The zero position for the intracostal joint was set at a frame from the video with the maximum inhalation observed for each individual. Therefore, relative to the costovertebral and sternocostal JCSs, the absolute intracostal angle values are less comparable among individuals.

Journal of Experimental Biology (2016) 219, 404-411 doi:10.1242/jeb.127928

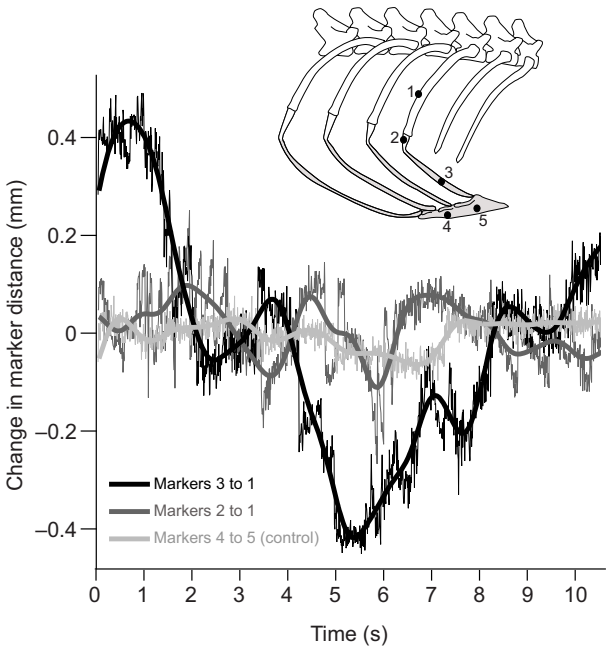

Fig. 5. Relative motion of vertebral and sternal rib segments during a representative deep breath. Raw and filtered inter-marker distance traces are shown (mean marker tracking precision for this study is ±0.1 mm). The change in distance between radio-opaque markers 3 and 1 shows that the sternal rib moves relative to the vertebral rib during breathing (expiration switches to inspiration at 5.4 s). The absence of detectable motion between markers 2 and 1 shows that the motion occurs at a thin cartilage flexion point ventral to the transition between bone and cartilage. *A priori* we expect no motion within the sternum, so the distance between markers 4 and 5 serves as a control.

the vertebral segment. Rotation around the *X*-axis indicates long-axis rotation of the sternal rib segment, and rotation around the *Y*-axis indicates depression–elevation of the sternal rib segment relative to the vertebral rib.

Breaths within and among individuals varied in duration, magnitude and mean rib posture. For comparison, breaths were zeroed to the mean angle for each rotational DOF and resampled to 100 points for expression as a percentage of the breathing cycle. To visualize the relative rotation from rostral to caudal in the cervical and vertebral rib series, we determined the maximum range of bucket-handle rotation observed for each individual in the cervical or vertebral ribs, i.e. the single greatest value observed in any of those ribs over all breaths for that individual. We then normalized the range of rotation for all cervical and vertebral ribs by that mean maximum range. The same procedure was followed for the sternal ribs, normalizing by the mean maximum range of motion across all the sternal ribs for each individual.

Precision

The precision of marker tracking *in vivo* can be measured from pairs of markers embedded in a rigid bone (Brainerd et al., 2010; Dawson et al., 2011; Tashman and Anderst, 2003). The distance between two markers embedded within a rigid bone is expected to be constant, but the apparent distance contains noise (e.g. Fig. 5, markers 4–5). Therefore, the standard deviation of inter-marker distance is a measure of marker-tracking precision. Marker-tracking precision *in vivo* for this study ranged from 0.006 to 0.017 mm across all co-osseous pairs of markers, with a mean of 0.011 mm.

The precision of six DOF motions at joints cannot be determined directly from marker-tracking precision. The precision of rigid-body motion depends on the 3D distribution of markers within the skeletal elements and the placement of the JCS. In this study, the precision of rigid-body motion was measured from a frozen specimen with markers in place. We translated and rotated the specimen in the X-ray beams, tracked the markers in the resultant videos, animated the bones, and measured the six DOF joint movements using the JCSs described above. In a frozen specimen, the bones do not move relative to each other. Therefore, all joint translations and rotations are expected to be zero, and the standard deviation of the JCS output is a measure of rigid-body precision (Menegaz et al., 2015). We found the mean precision for costovertebral joint translations along the *X*-, *Y*- and *Z*-axes to be 0.22, 0.24 and 0.04 mm, respectively. Precision for joint rotations around the *X*-, *Y*- and *Z*-axes was 1.46, 0.48 and 1.64 deg, respectively.

RESULTS

Costal anatomy and intracostal mobility

The presacral axial skeleton of *I. iguana* consists of eight cervical vertebrae and 16 dorsal vertebrae. The first four cervical vertebrae do not carry ribs, and cervical ribs 1 and 2 (on cervical vertebrae 5 and 6) are short. The third and fourth cervical ribs are well developed with a bony proximal part and a short cartilaginous plug at the distal tip (Fig. 1D). The serratus ventralis muscle sends muscle slips from the first three cervical ribs to the medial aspect of the scapula, but shows no connections to the fourth cervical rib (Carrier, 1989, 1990).

The first four dorsal ribs articulate with the sternum and consist of two parts: an osseous vertebral rib and a cartilaginous sternal rib (Fig. 1D). The bone of the vertebral rib articulates with a thick plug of cartilage, and then the cartilage narrows down to a putative zone of flexion, called here the ‘elbow’. The sternal ribs appear to be well mineralized, based on their appearance in videofluoroscopy and CT scans.

Prior to starting the XROMM animation process, we had to determine whether measurable bending occurred within the vertebral and sternal rib segments, and whether motion between the vertebral and sternal ribs occurred at the elbow, at the actual border between cartilage and bone, or perhaps not at all. These data were necessary to determine whether we should model the entire rib as one rigid body, the vertebral and sternal ribs as articulating rigid bodies, or the ribs as flexible along their full lengths.

We found that the vertebral ribs and the part of the sternal ribs ventral to the elbow do indeed act as rigid bodies, and motion between them occurs at the elbow. Pairwise distances between markers showed no measurable relative motion between the vertebral rib and the short cartilaginous plug dorsal to the elbow (Fig. 5, markers 1 and 2). The small fluctuations between markers 1 and 2 are within our marker tracking precision for this study (±0.1 mm), and we saw no consistent pattern of these fluctuations across breaths. Thus, the vertebral rib and the cartilage plug can be treated as one rigid body for XROMM animation. By contrast, we found relatively large distance changes between the cartilaginous plug and the sternal rib (Fig. 5, markers 2 and 3), indicating intracostal flexion at the elbow. Distance fluctuations between markers within the sternal ribs were also within our ±0.1 mm precision, indicating that the sternal ribs can be treated as rigid bodies (data not shown).

We also checked the rigid-body assumptions after animating our models. In Maya, the animated bones were visually checked against the original X-ray video to see whether the animated bone movements match the movements in the X-ray. For Ig03 and

Journal of Experimental Biology (2016) 219, 404-411 doi:10.1242/jeb.127928

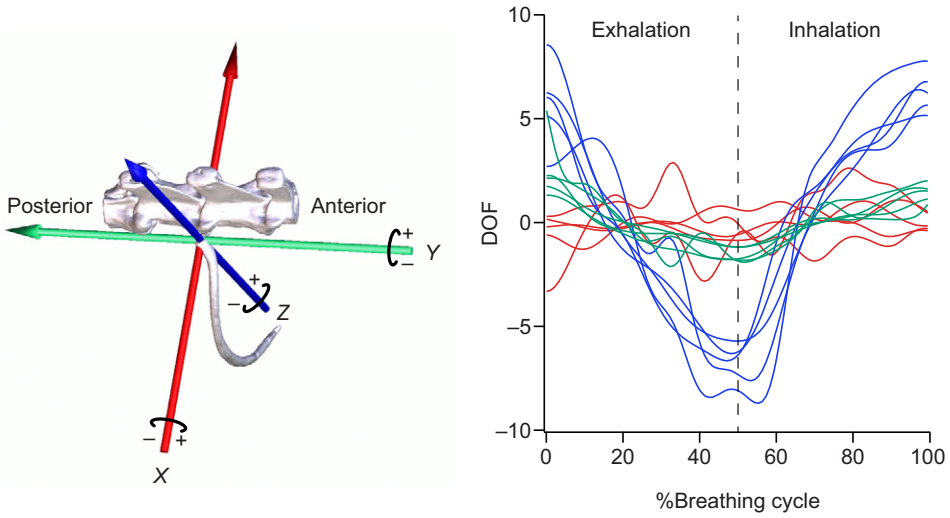

Fig. 6. Euler angle rotations at the costovertebral joint of the first vertebral rib (V1) over five breaths in one individual (Ig04). The angles were zeroed at their mean values and durations were normalized to 100%. The primary motion is bucket-handle rotation about a ventrodorsally oriented *Z*-axis (blue), with a small amount of caliper motion about a rostrocaudally oriented *Y*-axis (green). Red: pump-handle rotation.

Ig05, where some or all bones were animated by Scientific Rotoscoping (Gatesy et al., 2010), no evidence of bending within the vertebral ribs and the part of the sternal ribs ventral to the elbow was found. We also did not see any motion at the junction between the vertebral rib and the cartilaginous plug, but we could see motion at the elbow. Hence, for this study, we define the vertebral rib to be the bony rib plus the cartilaginous plug dorsal to the elbow, and the sternal rib to be the cartilaginous rib ventral to the elbow. As we found that motion between vertebral and sternal rib segments occurs at the elbow, hereafter we call the elbow the intracostal joint.

3D kinematics of vertebral and sternal segments of the first dorsal rib

Motion of the first vertebral rib (V1) at the costovertebral joint was dominated by bucket-handle rotation, defined as rotation about a ventrodorsally oriented axis (*Z*-axis, blue) in our costovertebral JCS (Fig. 6; Movies 2, 3). The rib rotated caudad during exhalation, thereby folding back and decreasing the volume of the thorax, and rotated craniad during inhalation (polarity set by the right-hand rule with the thumb pointing in the direction of the axis arrowhead).

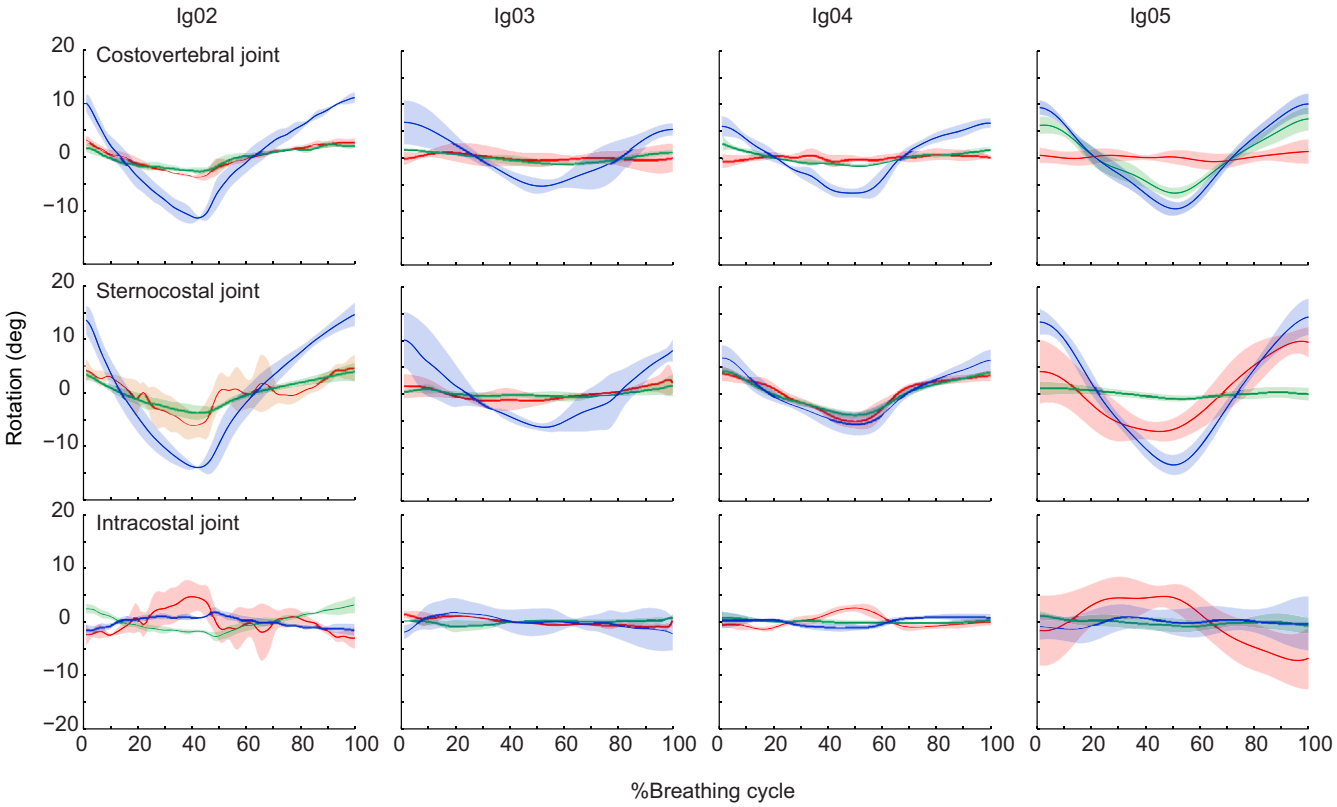

Fig. 7. Mean rotations of the three costal joints of the first dorsal rib in four individuals. See Materials and methods for a description of the JCSs. Each breath was defined as exhalation followed by inhalation. Angles were zeroed and time was normalized to 100%; solid lines show means (*N*=5 breaths per individual) and shading shows ±1 s.d. Costovertebral joint: blue, bucket-handle; green, caliper; red, pump-handle. Sternocostal joint: blue, bucket-handle; green, caliper (depression–elevation); red, long-axis rotation. Intracostal joint: blue, abduction–adduction; green, depression–elevation; red, long-axis rotation of the sternal rib.

Journal of Experimental Biology (2016) 219, 404-411 doi:10.1242/jeb.127928

Costovertebral motions in the other two rotational DOF, caliper (*Y*-axis, green) and pump-handle (*X*-axis, red), were much smaller than bucket-handle rotation in most individuals (Fig. 7; Table S1). The exception is Ig05, in which the costovertebral caliper approached bucket-handle amplitude, and a small amount of caliper motion was observed in all individuals. Discernible pump-handle motion was present only in Ig02, the animal with the deepest breaths (Fig. 7).

In the sternocostal joints of all four individuals, bucket-handle rotation was the dominant motion (Fig. 7; Table S2). Caliper motion and long-axis rotation were more variable. Long-axis rotation was observed in the first sternal rib of Ig02, Ig04 and Ig05 and in the second sternal rib of Ig02. In Ig02 and Ig04, caliper motion and long-axis rotation were almost equal in amplitude, whereas in Ig05, we found a larger amount of long-axis rotation and almost no caliper motion. In Ig03, both caliper motion and long-axis rotation were very small (Fig. 7; Table S2).

Rotations at the intracostal joints were relatively small in all four individuals (Fig. 7; Table S3). Long-axis rotation of the sternal rib relative to the vertebral rib was the dominant motion in individuals 2, 4 and 5 (Fig. 7), with positive rotation during the latter half of exhalation and negative rotation during inhalation, as defined by the polarity of the intracostal JCS (Fig. 4).

Motions in the three potential translational DOF were small in all joints (less than ±0.25 mm), and showed no patterns associated with breathing. Some small translations could be occurring at these joints, but they would be too small to detect in this study (rigid-body translation precision for marker-based XROMM in this study is about ±0.25 mm; see Materials and methods).

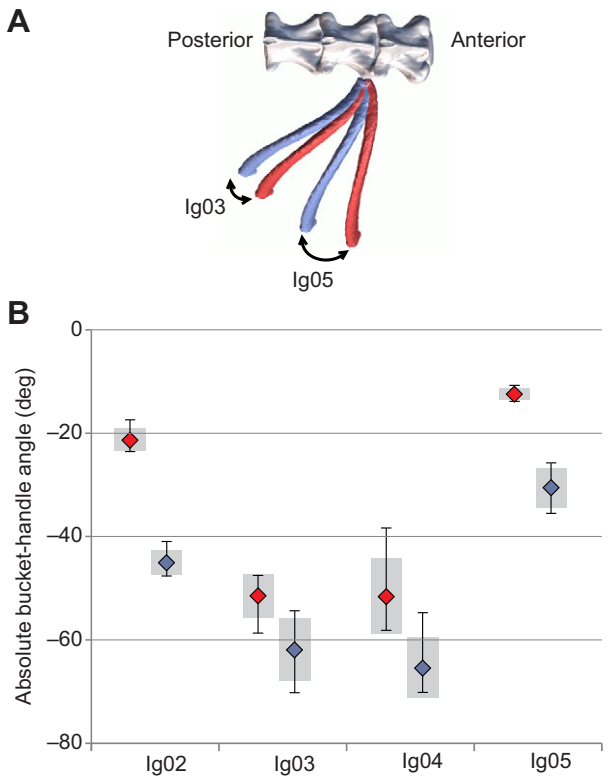

Fig. 8. Vertebral rib posture varies among individuals. The four iguanas centered their breathing motions on different positions within the potential range of bucket-handle angles. Ig02 and Ig05 tended to breathe around a more inhaled (inflated) posture. (A) Diagram of maximum inhaled (red) and exhaled (blue) postures of V1 for Ig03 and Ig05. (B) Box plot of bucket-handle rotation for V1 at maximum inhalation (red) and exhalation (blue) for each individual (*N*=5 breaths per individual). Mean angles across all trials are shown (diamonds); the whiskers indicate the range and the shaded boxes show ±1 s.d.

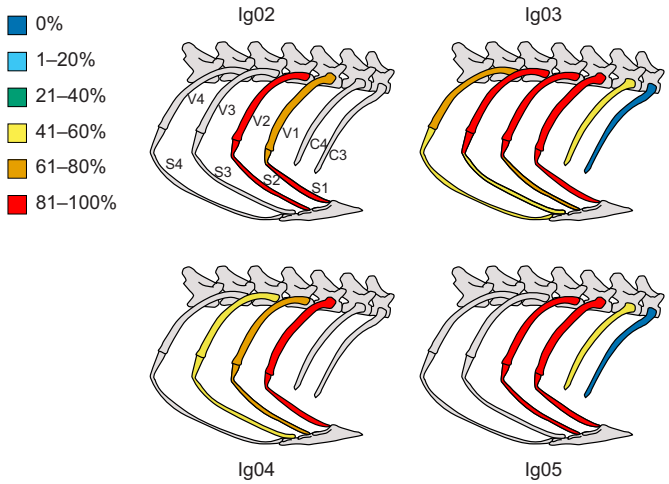

Fig. 9. Relative rotation of cervical, vertebral and sternal ribs in four green iguanas. The primary (bucket-handle) rotation for the costovertebral and sternocostal joints is shown. Absolute mean values (in degrees) for all rotations are in Table S1. Relative magnitudes in this figure are expressed as mean percentage of the maximum range of motion for each individual over five breaths in the cervical and vertebral or sternal rib series. Not all ribs were animated in all individuals (ribs not animated are gray).

The results presented above focus on the magnitude of rotations, i.e. the difference between maximum inhalation and exhalation, with the angles zeroed at their mean values (Figs 6, 7). This zeroing facilitates the display of means across breaths, but it obscures variation among individuals in the actual rib postures. When the rib angles are displayed relative to a standardized pose, in which 0 deg of bucket-handle rotation is defined as the vertebral rib positioned perpendicular to the vertebral column, the variations in rib posture become clear (Fig. 8). Our four iguanas centered their breathing motions on different positions within the potential range of bucket-handle angles: Ig02 and Ig05 tended to breathe around a more inhaled (inflated) posture. Indeed, mean exhaled postures in Ig02 and Ig05 (−45.0 and −30.5 deg) were closer to zero than the mean inhaled postures in Ig03 and Ig04 (−51.4 and −51.6 deg). Individuals 3 and 4 also showed more variation in the range of rib postures at both maximum inhalation and maximum exhalation (ranges of about 15–20 deg versus 5–10 deg in Ig02 and Ig05).

Variation of bucket-handle rotation along the rib cage

Given our finding that bucket-handle rotation dominated the motion of both the vertebral and sternal segments of the first dorsal rib (V1, S1), we focused on bucket-handle rotation for further analysis of how rib motion varies from rostral to caudal. We did not place markers in cervical ribs C1 and C2, but it was clear from the X-ray videos that these ribs do not move during the deep breaths analyzed here. We did rotoscope C3 and C4 in Ig03, and marked them in Ig04. We found no measurable motion in C3, but fairly large bucket-handle rotation in C4 (Fig. 9; Table S1). The most rostral dorsal ribs rotated substantially more than C4. The largest amount of bucket-handle motion was observed in V1 and V2 of all four individuals, and decreased caudally (Fig. 9; Table S1). Sternal ribs also showed a decrease in bucket-handle motion from cranial to caudal. In Ig02 and Ig05, the decrease in motion was not very

Journal of Experimental Biology (2016) 219, 404-411 doi:10.1242/jeb.127928

pronounced, with almost equal amounts of movement between S1 and S2. In Ig03 and Ig04, the decrease in motion was more pronounced, with S1 moving substantially more than the more caudal sternal ribs (Fig. 6; Table S1).

DISCUSSION

As in most squamates, the costovertebral joints of green iguanas are simple, hemispheric joints that potentially allow motion in all three rotational DOF (Fig. 1). However, the actual motions of the vertebral rib segments for breathing are concentrated into just one DOF, and vary little within or among individuals (Figs 6, 7). Bucket-handle rotation of the vertebral ribs dominates, with mean rotation exceeding 20 deg in our deepest breathing individual (Ig02; Fig. 7). Only one individual showed substantial rotation about a different axis, with Ig05 showing some pump-handle as well as bucket-handle rotation (Fig. 7). The costovertebral joint morphology does not constrain motion, so the musculature and connective tissues of the rib cage must be directing rib motion to produce such consistent motions within and among individuals.

The osseous vertebral rib segments connect ventrally to a cartilaginous plug, and thence via a thin elbow of cartilage to broader cartilaginous sternal ribs (Fig. 1). As predicted from this morphology, the vertebral and sternal ribs do not deform during breathing (Fig. 5). However, there is measurable motion at the thin elbow of cartilage connecting the vertebral and sternal rib segments (Fig. 5), and therefore we call this elbow the intracostal joint. Motion at the intracostal joint is, however, quite small, with about five degrees of long-axis rotation of the sternal rib relative to the vertebral rib in our deepest breathing individuals (Ig02 and Ig05; Fig. 7). This long-axis rotation of the sternal ribs is also evident at the sternocostal joints, where we also found substantial bucket-handle rotation, in concert with the motion of the vertebral ribs (Fig. 7).

The four iguanas in this study did not all breathe equally deeply, nor did they breathe within the same range of rib postures (Fig. 8). The depth of breaths reflects our methods for inducing deep breathing: in Ig02 and Ig05, the breaths were recorded immediately after trackway and treadmill exercise, respectively, whereas for Ig03 and Ig04, we relied just on the moderately deep breathing induced by handling the animals and placing them into the X-ray enclosure. One might expect that more shallow breathing would occur within a subset of the range of vertebral rib angles for deeper breaths, but that was not the case. Our two shallow breathers, Ig03 and Ig04, used a range of rib angles that were all more adducted (angles closer to −90 deg) than the range of our two deeper breathers (Fig. 8). Presumably, this means that the more shallow breathers had less air in their lungs, and a lower functional residual capacity, as well as a smaller tidal volume. These differences in vertebral rib posture were not correlated with differences in overall body posture, as all animals were standing up on their forelimbs with their sterna off the ground for the analyzed trials.

The foregoing discussion has focused on the kinematics of the first dorsal rib, as generally representative of the patterns of bucket-handle, pump-handle and caliper motion we observed (Table S1). However, the magnitude of rotation was not constant among cervical and vertebral ribs, but rather there was a pattern of increasing and then decreasing bucket-handle rotation from rostral to caudal (Fig. 9). We found that C1–C3 were held immobile, followed by an increase in bucket-handle rotation from C4 to V1, and roughly equal mean rotation of V1 and V2, but with individual animals and breaths showing patterns of V2 greater or less than V1. Caudal to V2, we found a gradient of decreasing bucket-handle rotation in V3 and more caudal ribs (Fig. 9). This pattern is consistent with our finding that the serratus ventralis muscle connects C1–C3 to the scapula, thus anchoring these cervical ribs to the pectoral girdle. In contrast, the serratus ventralis does not attach to C4, and we do see substantially greater motion in C4 (Fig. 9). The result of these gradients in bucket-handle rotation is a decrease in width of the intercostal spaces between C4 and V1, V1 and V2, and sometimes V1 and V2 during inhalation, and an increase in width of the more caudal intercostal spaces. This finding suggests that shortening of the intercostal muscles in these rostral spaces may contribute to inhalation by shifting the whole rib cage rostrad toward the stabilized cervical ribs C1–C3. The function of the intercostal muscles in spaces C4–V2 for inhalation is supported by a prior finding of consistent electrical activity in these rostral intercostal spaces, but not in more caudal intercostal spaces, during inhalation (Carrier, 1989).

Despite these differences in the magnitude of rotation, the 3D motion patterns of the ribs in green iguanas during breathing are remarkably consistent within and among individuals. Iguanas clearly do not need bicapitate ribs and complex costovertebral joints to constrain their motion to one primary axis, as is seen in other amniote groups (Claessens, 2009a,b; De Troyer et al., 2005). The unicapitate ribs and simple costovertebral joints of squamates are derived relative to the primitive condition of bicapitate ribs, so what might have been the selective advantage, if any, of these simpler, less restrictive joints in the evolution of Squamata? Green iguanas have recently been shown to have unidirectional flow in their lungs, joining alligators and varanid lizards as non-avian examples of unidirectional flow (Cieri et al., 2014; Farmer, 2015; Farmer and Sanders, 2010; Schachner et al., 2014). Perhaps some of the subtle differences in 3D motion along the rib cage reported here may assist the generation of unidirectional flow, but testing this hypothesis will require further analysis with a focus on regional volume changes.

Ribs also serve many other mechanical functions, in addition to breathing, such as body support and locomotion (Carrier, 1991; Claessens, 2015). Perhaps bicapitate rib morphology in non-squamate amniotes serves to stiffen the trunk for locomotion by preventing rotation around all axes except the one required for breathing. Unicapitate ribs allow the large changes in body shape seen in many squamates, such as flattening for basking in the sun and puffing up for defense (Deban et al., 1994). Unicapitate ribs may also be an exaptation for macrophagy in snakes, but clearly unicapitate ribs evolved at the base of Squamata, well before macrophagy (Hoffstetter and Gasc, 1969). Hence, the evolution of simple costovertebral joints and unicapitate ribs in squamates remains a bit of a puzzle. These permissive joints are not required for the stereotyped, hinge-like breathing motions we observed in this study, and the selective advantage, if any, of this costovertebral joint morphology in the evolutionary history of Squamata remains unclear.

Acknowledgements

We thank A. Sullivan, K. Devlin, M. Dawson, A. Camp, H. Astley and E. Tavares for assistance with animal husbandry, surgeries, data collection and analysis. We thank D. Moore and the Department of Diagnostic Imaging at Rhode Island Hospital for assistance with the CT scanning, and S. Gatesy and D. Baier for Maya MEL scripts and assistance with Scientific Rotoscoping.

Competing interests

The authors declare no competing or financial interests.

Author contributions

E.L.B. and D.A.R. conceived and designed the study, D.A.R. developed the surgical techniques, D.A.R. and S.M. performed the surgeries, D.A.R., E.L.B. and S.M. collected the data, S.M. analyzed the data and made the figures, E.L.B. and S.M. wrote the manuscript, and all authors reviewed and approved the manuscript.

Funding
This work was supported by the Bushnell Research and Education Fund and the US National Science Foundation [grant numbers 1120967, 1262156].

Supplementary information
Supplementary information available online at
http://jeb.biologists.org/lookup/suppl/doi:10.1242/jeb.127928/-/DC1

References

Baier, D. B., Gatesy, S. M. and Dial, K. P. (2013). Three-dimensional, high-resolution skeletal kinematics of the avian wing and shoulder during ascending flapping flight and uphill flap-running. *PLoS ONE* **8**, e63982.
Brainerd, E. L. (2015). Major transformations in vertebrate breathing mechanisms. In *Great Transformations in Vertebrate Evolution* (ed. K. P. Dial, N. Shubin and E. L. Brainerd), pp. 47-62. Chicago: Chicago University Press.
Brainerd, E. L. and Owerkowicz, T. (2006). Functional morphology and evolution of aspiration breathing in tetrapods. *Respir. Physiol. Neurobiol.* **154**, 73-88.
Brainerd, E. L., Baier, D. B., Gatesy, S. M., Hedrick, T. L., Metzger, K. A., Gilbert, S. L. and Crisco, J. (2010). X-ray Reconstruction of Moving Morphology (XROMM): precision, accuracy and applications in comparative biomechanics research. *J. Exp. Zool.* **313A**, 262-279.
Carrier, D. R. (1989). Ventilatory action of the hypaxial muscles of the lizard *Iguana iguana*: a function of slow muscle. *J. Exp. Biol.* **143**, 435-457.
Carrier, D. R. (1990). Activity of the hypaxial muscles during walking in the lizard, *Iguana iguana*. *J. Exp. Biol.* **152**, 453-470.
Carrier, D. R. (1991). Conflict in the hypaxial musculo-skeletal system: documenting an evolutionary constraint. *Amer. Zool.* **31**, 644-654.
Cieri, R. L., Craven, B. A., Schachner, E. R. and Farmer, C. G. (2014). New insight into the evolution of the vertebrate respiratory system and the discovery of unidirectional airflow in iguana lungs. *Proc. Natl. Acad. Sci. USA* **111**, 17218-17223.
Claessens, L. P. A. M. (2009a). A cineradiographic study of lung ventilation in *Alligator mississippiensis*. *J. Exp. Zool. A Ecol. Genet. Physiol.* **311A**, 563-585.
Claessens, L. P. A. M. (2009b). The skeletal kinematics of lung ventilation in three basal bird taxa (emu, tinamou, and guinea fowl). *J. Exp. Zool. A Ecol. Genet. Physiol.* **311A**, 586-599.
Claessens, L. P. A. M. (2015). Anatomical transformations and respiratory innovations of the archosaur trunk. In *Great Transformations in Vertebrate Evolution* (ed. K. P. Dial, N. Shubin and E. L. Brainerd), pp. 91-106. Chicago: Chicago University Press.
Dawson, M. M., Metzger, K. A., Baier, D. B. and Brainerd, E. L. (2011). Kinematics of the quadrate bone during feeding in Mallard ducks. *J. Exp. Biol.* **214**, 2036-2046.
De Troyer, A., Kirkwood, P. A. and Wilson, T. A. (2005). Respiratory action of the intercostal muscles. *Physiol. Rev.* **85**, 717-756.
Deban, S. M., O'Reilly, J. C. and Theimer, T. (1994). Mechanism of defensive inflation in the chuckwalla, *Sauromalus obesus*. *J. Exp. Zool.* **270**, 451-459.
Farmer, C. G. (2015). Unidirectional flow in lizard lungs: a paradigm shift in our understanding of lung evolution in Diapsida. *Zoology* **118**, 299-301.
Farmer, C. G. and Sanders, K. (2010). Unidirectional airflow in the lungs of alligators. *Science* **327**, 338-340.
Gatesy, S. M., Baier, D. B., Jenkins, F. A. and Dial, K. P. (2010). Scientific Rotoscoping: a morphology-based method of 3-D motion analysis and visualization. *J. Exp. Zool.* **313A**, 244-261.
Hoffstetter, R. and Gasc, J. P. (1969). Vertebrae and ribs of modern reptiles. In *Biology of the Reptilia*, Vol. 1 (ed. C. Gans, C. Bellairs and T. Parsons) pp. 201-310. London: Academic Press.
Kambic, R. E., Roberts, T. J. and Gatesy, S. M. (2014). Long-axis rotation: a missing degree of freedom in avian bipedal locomotion. *J. Exp. Biol.* **217**, 2770-2782.
Menegaz, R. A., Baier, D. B., Metzger, K. A., Herring, S. W. and Brainerd, E. L. (2015). XROMM analysis of tooth occlusion and temporomandibular joint kinematics during feeding in juvenile miniature pigs. *J. Exp. Biol.* **218**, 2573-2584.
Miranda, D. L., Schwartz, J. B., Loomis, A. C., Brainerd, E. L., Fleming, B. C. and Crisco, J. J. (2011). Static and dynamic error of a biplanar videoradiography system using marker-based and markerless tracking techniques. *J. Biomech. Eng.* **133**,121002.
Osmond, D. G. (1985). Functional Anatomy of the Chest Wall. In *The Thorax*, *vol. Part A* (ed. C. Roussos and P. T. Macklem), pp. 199-233. New York: Marcel Dekker, Inc.
Romer, A. S. (1956). *Osteology of the Reptiles*. Chicago: University of Chicago Press.
Schachner, E. R., Cieri, R. L., Butler, J. P. and Farmer, C. G. (2014). Unidirectional pulmonary airflow patterns in the savannah monitor lizard. *Nature* **506**, 367-370.
Tashman, S. and Anderst, W. (2003). In-vivo measurement of dynamic joint motion using high speed biplane radiography and CT: application to canine ACL deficiency. *J. Biomech. Eng.* **125**, 238-245.